Acta Cryst C STRUCTURAL CHEMISTRY
ISSN 2053-2296

# Zirconia-supported 11-molybdovanadophosphoric acid catalysts: effect of the preparation method on their catalytic activity and selectivity

Bouchra El Bakkali,[a] Guido Trautwein,[a] Juan Alcañiz-Monge[a]* and Santiago Reinoso[b]

[a]Grupo de Materiales Carbonosos y Medio Ambiente, Departamento de Química Inorgánica, Facultad de Ciencias, Universidad de Alicante, PO Box 99, Alicante 03080, Spain, and [b]Institute for Advanced Materials (InaMat), Universidad Pública de Navarra (UPNA), Edificio Jerónimo de Ayanz, Campus de Arrosadia, Pamplona 31006, Spain. *Correspondence e-mail: jalcaniz@ua.es

Received 5 May 2018
Accepted 14 September 2018

Edited by J. R. Galán-Mascarós, Institute of Chemical Research of Catalonia (ICIQ), Spain

**Keywords:** polyoxometalates; heterogeneous catalysts; oxidation catalysis; adamantane; crystal structure.

**Supporting information**: this article has supporting information at journals.iucr.org/c

The oxidation of adamantane with hydrogen peroxide catalyzed by zirconia-supported 11-molybdovanadophosphoric acid is shown to be a suitable green route for the synthesis of adamantanol and adamantanone. This work evaluates how the catalyst activity and selectivity are affected by some of its preparative parameters, such as the method for supporting the catalytically active heteropoly acid over the zirconia matrix or the pretreatments applied to the resulting materials before being used as heterogeneous catalysts. Our results indicate that the most effective catalysts able to maintain their activity after several reaction runs are those prepared by following the sol-gel route, whereas the most selective catalysts are those obtained by impregnation methods. Moreover, the calcination temperature has also been identified as a relevant parameter influencing the performance of catalysts based on supported heteropoly acids. The increasing catalytic activity observed over several consecutive reaction runs has been attributed to the formation of peroxo derivatives of polyoxometalate clusters at the surface of the catalyst and their accumulation after each reaction cycle.

## 1. Introduction

Fine chemicals constitute a thriving sector of the chemical industry that comprises the production of complex molecules with high added value and widespread use in fields such as pharmaceuticals, cosmetics or food additives (Noyori *et al.*, 2003; Shaabani & Rezayan, 2007). Most of these molecules are obtained from elaborate synthetic routes involving organic reactions carried out in the liquid phase, which usually require catalysts for the reactions to proceed (Arichi *et al.*, 2008). Classical Lewis acids (*e.g.* $AlCl_3$, $BF_3$, $SnCl_4$ or $TiCl_4$) are among the most extensively used examples of such catalysts (Pizzio *et al.*, 1998; Parida & Mallick, 2008; Rivera *et al.*, 2012). These acids are characterized by their remarkable affinity toward highly electronegative atoms, oxygen and nitrogen in particular, thus possessing the ability to activate the functional groups of organic substrates. To increase their selectivity, catalytic activity and/or stereochemistry in synthetic organic reactions, Lewis acids are further tuned through combination with different ligands to form new custom-designed catalysts based on metal complexes and/or metal salts (Popa *et al.*, 2006; Bordoloi *et al.*, 2007; Rao *et al.*, 2010). The interest in using such catalysts with Lewis acid character for synthetic organic chemistry lies in their versatility in a wide range of reactions, including Diels–Alder cycloadditions, Friedel–Crafts alkyl-

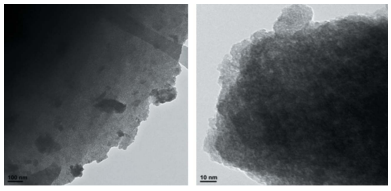

ations/acylations, aldol condensations, Michael additions, chain isomerizations, or oxidations such as epoxidation and dehydrogenation (Boon *et al.*, 1986; Wang *et al.*, 2001; Pizzio *et al.*, 2003; Chang *et al.*, 2010; Qiu *et al.*, 2015).

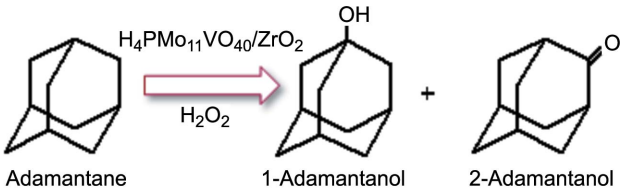


Scheme 1

The latter oxidation reactions require reagents capable of donating O atoms to the catalyst–substrate adduct, which coordinate to the metal centres with Lewis acidity to form oxometallic or peroxometallic intermediate species, and then transfer to the substrate leading to the oxidized product (Shinachi *et al.*, 2005). In this regard, one of the most relevant advances undergone by oxidation catalysis is the increased use of cheaper and less environmentally harmful oxidants, such as hydrogen peroxide ($H_2O_2$), the reduction product of which is merely water in contrast to other inorganic oxidants that give rise to the formation of pollutants (Bossmann *et al.*, 1998). As $H_2O_2$ usually lacks enough activity because of its low decomposition temperature, catalysts are required to raise the reaction rates (Babou *et al.*, 1995), among which transition-metal-containing molecular species (*e.g.* Ti, V, Mo, W, Cr, Mn, Fe and Re) stand out as the most suitable because their ease in forming oxo- or peroxometallic derivatives gives them excellent activities and selectivities in $H_2O_2$-based oxidation reactions. However, two major drawbacks are associated with such transition-metal-based molecular catalysts. On the one hand is their marked tendency to undergo deactivation through oligomerization, which leads to polynuclear oxo-bridged complexes that are catalytically inactive. On the other hand is the fact that they are usually soluble in the reaction medium, which makes the catalytic processes run in the homogeneous phase when the optimization of such processes from the industrial viewpoint demands insoluble solid catalysts able to work under heterogeneous conditions.

These two major drawbacks can be overcome by making the molecular catalysts insoluble in the reaction medium and, therefore, the development of new solid acid catalysts with high selectivity has become a focus of attention in catalysis, as indicated by the remarkable number of scientific studies produced on this topic in recent decades. One elegant approach to the design of such a type of heterogeneous catalyst is seen in so-called heterogenization, that is, the immobilization of soluble species as the catalytically active functionalities on a solid support that provides a heterogeneous character to the resulting material. Supported catalysts are of great interest because of their many advantages, including their facile separation from the reaction products, which avoids any potential contamination of the latter, and the possibility of recycling and reusing the catalysts in consecutive reaction runs (Leofanti *et al.*, 1998; Farhadi & Zaidi, 2009; Alcañiz-Monge *et al.*, 2014). The selection of the appropriate support is a critical aspect because, depending on the type of catalytically active species, the support can strongly affect, enhance or reduce both its selectivity and/or its activity. This fact has been theoretically analyzed in terms of strong metal–support interactions (SMSI) (Tauster *et al.*, 1978; Goodman, 1995) and, recently, also in terms of electronic metal support interactions (EMSI) (Campbell, 2012). The basic concept behind both SMSI and EMSI is that the chemical bonding required to anchor the catalyst to the support can change the electronic and/or chemical structure of the former, hence modifying its catalytic behaviour.

Heteropoly acids (HPAs) stand out as one class of molecules with the highest potential to catalyse the $H_2O_2$-based oxidation of organic substrates efficiently. The large family of family of anionic metal–oxygen clusters known as polyoxometalates (POMs) comprises a number of species with very diverse compositions, shapes and sizes (Pope & Müller, 1991) and HPAs specifically refer to the protonated forms of the subclass of heteropolyanions, which incorporate additional elements (heteroatoms) in geometrically well-defined central sites (tetrahedral or octahedral) besides oxygen and metals from groups 5 and 6. A thorough body of reports on the catalytic applications of POM species can be found in the literature (Kozhevnikov, 2002), many of which refer to the $H_n[XM_{12-x}M'_xO_{40}]$ HPAs, with the well-known Keggin-type structure as the most relevant representatives ($X$ = heteroatom; *e.g.* $Si^{IV}$ or $P^V$; $M$ or $M'$ = $Mo^{VI}$, $W^{VI}$ or $V^V$). As HPAs show high solubility in a range of polar solvents, they need to be immobilized on porous solid matrices for application as supported catalysts under heterogeneous conditions, and different supports have been successfully explored to this end, such as mesoporous MCM-41 silica (Tropecêlo *et al.*, 2010), zirconia (Alcañiz-Monge *et al.*, 2018), activated carbonaceous materials (Alcañiz-Monge *et al.*, 2013) or alumina (Endalew *et al.*, 2011).

Here we report our studies on the applicability of a series of HPA-immobilized porous solids as heterogeneous acid catalysts for the green oxidation of organic substrates with $H_2O_2$ as an eco-friendly oxidant. In a previous work (Martín-Caballero *et al.*, 2016), we tested the catalytic activity of some HPA species (*i.e.* $H_3[PMo_{12}O_{40}]$ and $H_4[PVMo_{11}O_{40}]$ in a homogeneous phase), as well as that of $V_2O_5$, toward the oxidation of adamantane using $H_2O_2$ as oxidant (see Scheme 1), and found that the $H_3[PMo_{12}O_{40}]$ species, which is a well-established oxidation catalyst for a range of organic substrates (Mizuno & Kamata, 2011; Kozhevnikov, 2002), was in fact remarkably inactive under our conditions. The replacement of molybdenum(VI) centres with vanadium(V) atoms in the Keggin-type framework has proven to be beneficial for redox catalysis as it enhances the redox character of the POM cluster (Molinari *et al.*, 2011) and, accordingly, we obtained high conversions instead (90%) by using the vanadium(V)-monosubstituted $H_4[PVMo_{11}O_{40}]$ derivative (hereafter referred to as **VPMo**). Following on from these studies, the **VPMo** species has been selected in this work as the catalytically active probe molecule among the different Keggin-type HPAs that have been reported to date. Zirconia ($ZrO_2$, hereafter abbreviated

as **Z**) has been chosen as the porous solid matrix for immobilizing the **VPMo** clusters because of the strong interactions toward oxo–molybdic species that this oxide is able to establish. Considering the comments above on the SMSI and EMSI effects, we have analysed in this work the influence exercised on the catalytic properties of the **VPMo** cluster by interaction with different **Z** supports. The **Z**-supported heterogeneous catalysts have been prepared following two different synthetic approaches that differ in the procedure through which the support is obtained: (i) wet-impregnation, in which **Z** is first obtained by co-precipitation methods and then impregnated with **VPMo** solutions, and (ii) sol-gel, in which the **VPMo** clusters are directly integrated into the **Z** support, while the latter is being formed. Several *x***VPMo**/**Z***t* (impregnation) and *x***VPMo**/**ZG***t* (sol-gel denoted with **G**) heterogeneous catalysts with different HPA loadings (*x* = mass percentage of **VPMo** from 5 to 50 wt%) and thermal treatments (*t* = calcination temperature from 100 to 500 °C) have been prepared with the purpose of investigating any potential effect of the preparative method on their performance as oxidation catalysts (activity or selectivity). The oxidation of adamantane with hydrogen peroxide has been selected as the test reaction to probe the catalytic properties of our materials because substituted adamantane derivatives (adamantanol or adamantanone) are important precursors for drugs and photoresistant materials among other valuable products.

## 2. Experimental

### 2.1. Materials and methods

The $H_4PVMo_{11}O_{40}{\cdot}32H_2O$ heteropoly acid (**VPMo**) was synthesized following literature methods that involve extraction with diethyl ether of a mixture of sodium molybdate dihydrate ($Na_2MoO_4{\cdot}2H_2O$, 6.25 mmol in 12.5 ml of water), phosphoric acid ($H_3PO_4$, 6.25 mmol in 12.5 ml of hot water) and sodium *meta*-vanadate ($NaVO_3$, 69 mmol in 25 ml of water), followed by recrystallization from water of the solid product obtained from the resulting etherate fraction (Tsigdinos & Hallada, 1968). The **Z**-supported **VPMo** catalysts were prepared as follows:

*Impregnation method*: the **Z** support was firstly prepared by a precipitation process involving dropwise addition of an aqueous 0.1 *M* $NH_4OH$ solution to an aqueous 0.1 *M* solution of zirconyl dichloride ($ZrOCl_2{\cdot}8H_2O$) (3.2 g onto 100 ml) at room temperature with constant stirring until reaching a pH value of 10. The resulting hydrogel was aged at room temperature for 24 h, filtered under vacuum, washed thoroughly with distilled water until chloride free and dried in an oven at 100 °C for 24 h. The quantities of **VPMo** required to achieve POM loadings of 5, 10, 25 and 50 wt% were then dissolved in the minimum amount of water and added onto the dry support to form a slurry, which was subsequently placed in an oven at 100 °C to remove all water (for example, 0.25 g of **VPMo** were added to 0.75 g of **Z** to reach a POM loading of 25 wt%).

*Sol-Gel method*: the precursor zirconium(IV) *n*-butoxide $\{Zr[O(CH_2)_3CH_3]_4$; 3 ml, 7.3 mmol} was stirred in hot ethanol (60 °C, 10 ml) for 10 min until dissolution and the pH was adjusted to a value of 2 with concentrated HCl after cooling the resulting solution to room temperature. The required amount of **VPMo** to obtain a POM loading of 50 wt% (0.9 g) was then dissolved in a water–ethanol mixture (5/13 ml) and added dropwise to the above solution. The resulting mixture was allowed to stir at room temperature until formation of a gel, which was subsequently dried in vacuum at 100 °C for 24 h.

All catalysts obtained from both impregnation and sol-gel methods, as well as pristine **Z** samples prepared following the latter procedure but without addition of any **VPMo**, were calcined in air at temperatures between 100 and 500 °C for 2 h prior to full characterization and evaluation in the model catalytic test reaction.

### 2.2. Characterization of the catalysts

The crystal structure and particle morphology of the **Z**-supported **VPMo** catalysts synthesized in this work were examined by powder X-ray diffraction (PXRD) on a Seifert JSO Debye-Flex 2002 diffractometer (Cu *Kα* radiation) and by transmission electron microscopy (TEM) in a JEOL JEM-2010 equipment, respectively (Figs. S1–S3 in the supporting information). Fresh and recycled catalysts were comparatively analysed by further characterization techniques, such as diffuse reflectance IR Fourier transform spectroscopy (DRIFTS) and thermogravimetry (TGA). A Bruker RFS/100 spectrometer was used to record the DRIFT spectra of the samples as KBr pellets in the range 600–4000 $cm^{-1}$. A TA Instruments 2960 SDT thermobalance was used to carry out the TGA measurements from room temperature to 750 °C at a rate of 20 °C $min^{-1}$ under a 60 ml $min^{-1}$ flow of synthetic air.

The porous textures of the **Z** supports and the **Z**-supported **VPMo** catalysts were characterized by physical adsorption of gases using the equipment Autosorb 6-B ($N_2$ at −196 °C) or Autosorb-6 ($CO_2$ at 0 °C). The solid samples were degassed under vacuum at 100 °C for 4 h prior to performing the analyses. The specific surface area was determined from the Brunauer–Emmet–Teller (BET) equation (Brunauer *et al.*, 1938) and the volume of the micropores was calculated with the Dubinin–Radushkevich (DR) equation (Dubinin, 1966). The pore volumes were calculated as follows (Cazorla-Amorós *et al.*, 1996): (*a*) the volume of the ultramicropores ($V_{CO2}$, pore size < 0.7 nm) was estimated from the DR curves of the $CO_2$ adsorption experiments at relative pressures $P/P_0 <$ 0.015; (*b*) the total volume of the micropores ($V_{N2}$, pore size < 2 nm) was calculated from the DR curves of the $N_2$ adsorption experiments at relative pressures $P/P_0 < 0.14$; (*c*) the volume of the supermicropores (0.7 nm < pore size < 2 nm) was obtained from the difference between $V_{N2}$ and $V_{CO2}$; (*d*) the total porous volume ($V_T$) was estimated from the $N_2$ adsorption isotherm and, more specifically, from the amount adsorbed at relative pressures $P/P_0 = 0.99$; (*e*) the mesoporous

Table 1
Textural properties of *x***VPMo**/Z*t* catalysts obtained by the impregnation method.

| | $V_{N2}$ (cm$^3$ g$^{-1}$) | $V_{CO2}$ (cm$^3$ g$^{-1}$) | $V_T$ (cm$^3$ g$^{-1}$) | SBET (m$^2$ g$^{-1}$) |
|---|---|---|---|---|
| **Z** | 0.19 | 0.09 | 0.20 | 330 |
| 5**VPMo**/**Z**100 | 0.18 | 0.10 | 0.19 | 310 |
| 10**VPMo**/**Z**100 | 0.13 | 0.07 | 0.14 | 220 |
| 25**VPMo**/**Z**100 | 0.10 | 0.05 | 0.11 | 180 |
| 50**VPMo**/**Z**100 | 0 | 0 | 0 | 0 |
| 50**VPMo**/**Z**300 | 0 | 0 | 0 | 0 |

volume ($V_{meso}$, 2 nm < pore size < 50 nm) was calculated from the difference between $V_T$ and $V_{N2}$.

### 2.3. Catalytic tests

The **Z**-supported **VPMo** samples were tested as heterogeneous catalysts in the liquid-phase oxidation of adamantane with $H_2O_2$. This model reaction was carried out in a glass jacket (internal volume of 27 ml) placed inside a steel reactor (45 ml) coupled to a manometer to monitor the pressure of the reaction system. The glass jacket was filled with the substrate adamantane (25 mg, 0.184 mmol), acetonitrile as solvent (10 ml), $H_2O_2$ 30 wt% as oxidant (3 ml, 30 mmol), the corresponding catalyst (100 mg), a few drops of concentrated HCl and a Teflon stirring bar to homogenize the mixture. The oxidation reaction was allowed to run for 6 h at a thermostatically controlled temperature of 75 °C. The 50**VPMo**/**Z** and 50**VPMo**/**ZG** samples calcined at temperatures between 100 and 300 °C were selected to assess the reusability of our catalysts. These samples were recovered by filtration after the 6 h of reaction set for the catalytic test and reused in a new reaction run without any intermediate regeneration stage. This process was repeated through four successive catalytic cycles.

The nature of the reaction products was identified by gas chromatography coupled with mass spectrometry (GC–MS) on aliquots of 1 µl taken from the reaction solution upon completion of a given catalytic cycle ($t$ = 6 h). In addition, aliquots of 1 µl were also taken at each hour during the catalytic cycle ($t$ = 6 h) for the 50**VPMo**/**Z**100, 50**VPMo**/**Z**300 and 50**VPMo**/**ZG**300 samples. The equipment used for this purpose was an Agilent 6890 gas chromatograph fitted with an HP-5 column (30 × 250 × 0.25 µm) and coupled to an Agilent 5975 mass spectrometer with a quadrupole detector. Once all the reaction products had been identified, the conversion and distribution of the reaction products were quantitatively estimated from proper calibration procedures using the above GC equipment, but provided with a flame ionization detector (FID) and an HP-1 column (100% methylsiloxane, 30 × 250 × 0.25 µm). In both cases, the operating conditions for chromatography were as follows: injection temperature: 280 °C; split mode, flow ratio of 1:20; column flow: 1.6 ml min$^{-1}$ of He in constant flow mode; temperature program: 40 °C for 1 min, 25 °C min$^{-1}$ to 250 °C, isotherm for 5.6 min; air flow: 400 ml min$^{-1}$; $H_2$ flow: 40 ml min$^{-1}$.

To determine the extent of the **VPMo** leaching upon the oxidation reaction, the liquid media obtained after recovering the solid catalyst by filtration was subsequently analysed by UV–Vis spectroscopy using a JASCO UV–Vis/NIR V-670 spectrophotometer. Representative UV–Vis spectra of these analyses are displayed in Fig. S4 in the supporting information.

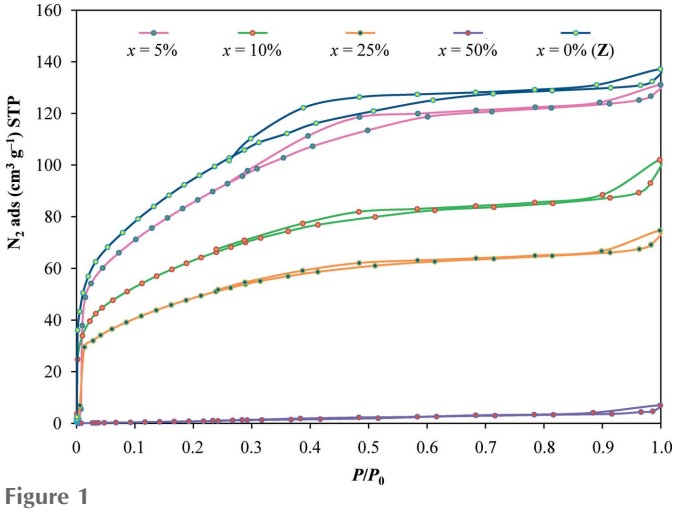


Figure 1
$N_2$ adsorption–desorption isotherms at −196 °C of the **Z** support and *x***VPMo**/**Z**100 catalysts ($x$ = 0–50 wt% of **VPMo**).

## 3. Results and discussion

### 3.1. Characterization of the catalysts obtained by the impregnation method

**3.1.1. Porous texture.** Fig. 1 shows the $N_2$ adsorption-desorption isotherms collected at −196 °C for the four **Z**-supported **VPMo** catalysts obtained by the impregnation method with POM loadings of 5, 10, 25 and 50 wt%, while Table 1 lists the values of the different parameters that define their textural properties, namely the BET surface area (SBET), the volume of the ultramicropores ($V_{CO2}$), the total microporous volume ($V_{N2}$) and the total porous volume ($V_T$), which have been calculated from the $N_2$ and $CO_2$ adsorption–desorption isotherms. All of the collected $N_2$ isotherms are of type I according to the IUPAC classification (Thommes *et al.*, 2015) and they show significant adsorption at low relative pressures ($P/P_0 < 0.2$) and comparatively much less adsorption at higher relative pressures ($P/P_0 > 0.3$), which is indicative of the character of our samples being mainly microporous with a subtle contribution of mesoporosity. The impregnation of the **Z** support with **VPMo** leads to a decrease in the porosity that becomes more pronounced as the POM loading increases. The adsorption capacity is retained nearly unmodified when the material is loaded with 5 wt% of **VPMo**, but it drops by 30% compared to the pristine **Z** support with a loading of just 10 wt% and is fully blocked for the 50**VPMo**/**Z** materials with the highest POM loading among the synthesized materials. Considering the lack of porosity displayed by the **VPMo** starting material (Moffat, 2001), the decrease in the adsorption capacity showed by our catalysts with increasing POM loading could, in principle, be attributed to the 'inert' weight with which the impregnated clusters contribute to the solid

sample. Moreover, the shape of the isotherms is also modified upon impregnation. The isotherm elbow observed at low pressures displays an open shape for the pristine **Z** support that is indicative of a wide distribution of micropore sizes, but it undergoes a continuous narrowing process as the POM loading increases, which reveals that impregnation gradually enhances the homogenization of the micropore sizes in the support.

According to the data listed in Table 1, the textural parameters remain nearly unaffected when the **Z** support is impregnated with 5 wt% of **VPMo**, most likely due to the clusters being supported at the outer surface of the zirconia nanoparticles upon impregnation. However, an additional loading of 5 wt% (10**VPMo**/**Z**100 sample) results in a significant reduction in the specific volume of the total microporosity ($V_{N2}$) that is less pronounced for the specific volume of the narrow micropores ($V_{CO2}$). This fact can only be explained by considering that the adsorption of the **VPMo** clusters takes place preferentially in the wide microporosity (pore size > 0.7 nm) and produces its partial block (Alcañiz-Monge *et al.*, 2008). This fact agrees well with what is observed for the adsorption of HPA species in activated carbonaceous supports, which has been shown to occur mainly in the supermicroporous domain. This result is also consistent with the average size of the Keggin-type POM clusters, which display diameters of 0.8–1.0 nm regardless of the addenda metal or heteroatom and hence they cannot be incorporated into the ultramicropores due to size exclusion (Song *et al.*, 2002).

**3.1.2. Powder X-ray diffraction**. Fig. 2 shows the PXRD patterns of the **Z** support, the **VPMo** heteropoly acid and the *x***VPMo**/**Z**100 catalysts with POM loadings of 5, 10, 25 and 50 wt%. The **Z** support obtained by co-precipitation displays a clear amorphous nature, most likely due to the low calcination temperature applied to the $Zr(OH)_4$ hydrogel formed in the course of such a synthetic procedure. The single remarkable feature of the diffraction pattern is the presence of a very broad band of low intensity that extends from 2$\theta$ values of 20 to 35° and is associated with the 111 reflection of the metastable tetragonal $ZrO_2$ phase [JCPDS 80-2155C]. In contrast, the **VPMo** starting material shows a well-defined diffraction pattern with a number of sharp and intense maxima that is characteristic of a compound with a high degree of crystalline order but fades away upon immobilizing the clusters at the support. New sharp diffraction maxima appear when the amount of impregnated **VPMo** is above 10 wt% and, although their heights increase with the POM loading, their intensities remain weak in all samples. This fact reveals that the **VPMo** clusters do not form large crystalline aggregates upon impregnation, but are highly dispersed over the surface of the **Z** support even for materials with a POM loading as high as 50 wt%. It is worth noting that the new diffraction maxima appearing for samples with POM loadings above 10 wt% do not correlate with any known crystalline phase of **VPMo**, which indicates that either the crystalline structure of the **Z**-supported **VPMo** differs from that of the starting material or the chemical nature of the cluster might be somehow modified upon impregnation.

The potential effect of thermal treatments on the structure of the **Z**-supported **VPMo** catalysts was also inspected through PXRD experiments on the pristine support and the sample with the highest content of **VPMo** (50**VPMo**/**Z**) calcined in air for 2 h at different temperatures between 100 and 400 °C (Fig. 3). For the **Z** support, our results show that the initial amorphous material gains significant crystallinity upon thermal treatment at 400 °C and is partially transformed into a monoclinic crystal phase (JCPDS 7-3430M). The presence of tetragonal $ZrO_2$ was identified from the diffraction maxima located at 2$\theta$ values of *ca* 30, 35 and 50°, which originate from the 101, 110 and 112 reflections, respectively. Partial formation of monoclinic $ZrO_2$ was confirmed from the diffraction maxima observed at 2$\theta$ values of *ca* 24, 28, 32, 42, 46, 54 and 56°, which correspond to the 011, 111, $\bar{1}11$, 121, 202, $\bar{2}02$ and 013 reflections, respectively. In the case of the 50**VPMo**/**Z***t* catalysts, calcination up to 300 °C does not appear to induce any remarkable structural modification in the

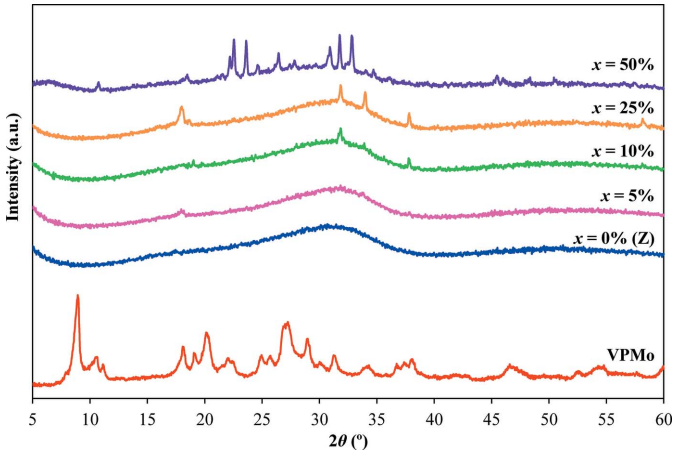


**Figure 2**
PXRD patterns of *x***VPMo**/**Z**100 samples (*x* = 0–50 wt% of **VPMo**).

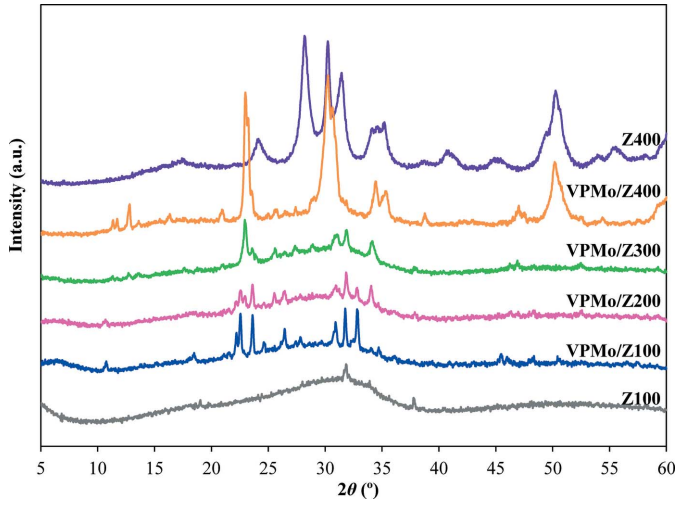


**Figure 3**
PXRD patterns of calcined 50**VPMo**/**Z***t* samples (*t* = 100–400 °C).

materials, but the diffraction pattern of 50**VPMo**/**Z**400 calcined at 400 °C is indeed substantially modified as additional new diffraction maxima are observed for this sample. These additional peaks are related in part with the crystallization of the **Z** support in the tetragonal phase, as commented on above (the presence of monoclinic $ZrO_2$ could not be detected in this case), but the appearance of a highly intense diffraction maximum at $2\theta = 23°$ corresponds to the formation of the $\beta$-type crystal phase of $MoO_3$ (Molinari *et al.*, 2011). This fact reveals that a significant fraction of the **VPMo** clusters, if not all, is thermally decomposed at 400 °C, which is consistent with what was reported by Schlögl and coworkers, who found that the **VPMo** starting material is thermally stable only at temperatures below 300 °C (Herzog *et al.*, 1997).

**3.1.3. Diffuse reflectance IR Fourier transform spectroscopy**. The DRIFT spectra of the **VPMo** starting material, the pristine **Z** support and the 50**VPMo**/**Z** catalysts calcined at 100 and 300 °C are compared in Fig. 4. The spectrum of the support shows two bands of strong intensity at about 1620 and 1350 $cm^{-1}$ that correspond to the H—O—H bending vibrations of physisorbed and crystallization water molecules, respectively (Patel *et al.*, 2003), together with a very broad signal centred at about 850 $cm^{-1}$ that can be attributed to the stretching vibrations of the Zr—O bonds in tetragonal $ZrO_2$ (Hernández Enríquez *et al.*, 2009). For the **VPMo** starting material, the spectrum is dominated by the fingerprint of the primary structure of a phosphomolybdate cluster of the Keggin-type (Mestl *et al.*, 2001): $\nu_{as}$(P—$O_a$) at 1070 $cm^{-1}$, $\nu_{as}$(Mo═$O_d$) at 980 $cm^{-1}$, $\nu_{as}$(Mo—$O_b$—Mo) at 912 $cm^{-1}$ and $\nu_{as}$(Mo—$O_c$—Mo) at 840 $cm^{-1}$, where $O_a$ is a central O atom, $O_d$ is a terminal oxide ligand, $O_b$ is a bridging O atom between corner-sharing $MoO_6$ octahedra and $O_c$ is a bridging O atom between edge-sharing $MoO_6$ octahedra. The bands of strong intensity located at 3500 [$\nu$(O—H)] and 1600 $cm^{-1}$ [$\delta$(H—O—H)] are assigned to the presence of water molecules in the secondary structure of the hydrated **VPMo** species (Arichi *et al.*, 2008; Shinachi *et al.*, 2005), whereas the representative signals originating from monosubstitution with vanadium(V) in the Keggin-type structure are partially masked by the $\nu_{as}$(P—$O_a$) and $\nu_{as}$(Mo═$O_d$) peaks as they appear at 1076 and 990 $cm^{-1}$ [$\nu_{as}$(V—$O_a$) and $\nu_{as}$(V═$O_d$), respectively].

In the case of the **Z**-supported **VPMo** catalysts, both samples display significant changes in the fingerprint associated with the primary structure of the Keggin-type clusters, which is in principle indicative of a good interaction between the **VPMo** species and the **Z** support. Two additional signals can be observed at 997 and 1037 $cm^{-1}$, and these can be related with the presence in our samples of $MoO_3$ and $V_2O_5$, respectively (Damyanova & Fierro, 1998; Dimitratos & Védrine, 2006). This fact reveals that the **VPMo** clusters are partially degraded with extrusion of the vanadium(V) centres during the synthesis of our catalysts by the impregnation method (Rocchiccioli-Deltcheff & Fournier, 1991; Mizuno *et al.*, 1996), which can be explained on the basis of the preparative procedure of the **Z** support involving its precipitation as a $Zr(OH)_4$ hydrogel under basic conditions (pH = 10). Literature reports on the stability of Keggin-type phosphomolybdate HPAs in aqueous solution (McGarvey & Moffat, 1991) have shown that this type of cluster is stable only under highly acidic conditions (pH < 2), and that they gradually degrade into other POM species through alkaline hydrolysis of *M*—O—*M* bonds as the pH increases (*e.g.* $[PMo_{11}O_{39}]^{7-}$ in the pH range 3–5 and $[HP_2Mo_5O_{23}]^{5-}$ in the pH range 5–6), in such a way that full breakdown of the cluster frameworks into simple oxoanions is achieved at pH > 6. These studies cannot be extrapolated to our system straightforwardly, but since impregnation of the basic **Z** support with the acidic **VPMo** must take place *via* interaction between the hydroxy groups of the $Zr(OH)_4$ hydrogel and protons of the HPA species, it is likely that this acid–base reaction causes partial hydrolysis of some of the clusters and subsequent alkaline degradation to some extent, which would be accompanied by extrusion of molybdenum(VI) and vanadium(V) atoms to form the corresponding oxides. From the thermal point of view, it has been suggested that the structural disorder

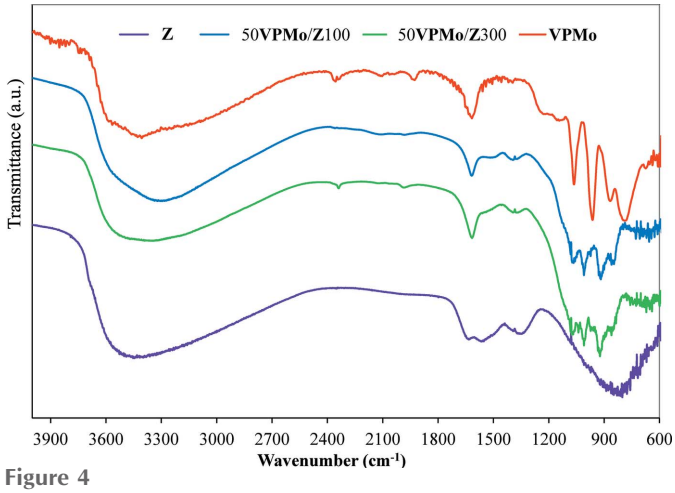


**Figure 4**
DRIFT spectra of **VPMo**, **Z** support and 50**VPMo**/**Z** samples calcined at 100 and 300 °C.

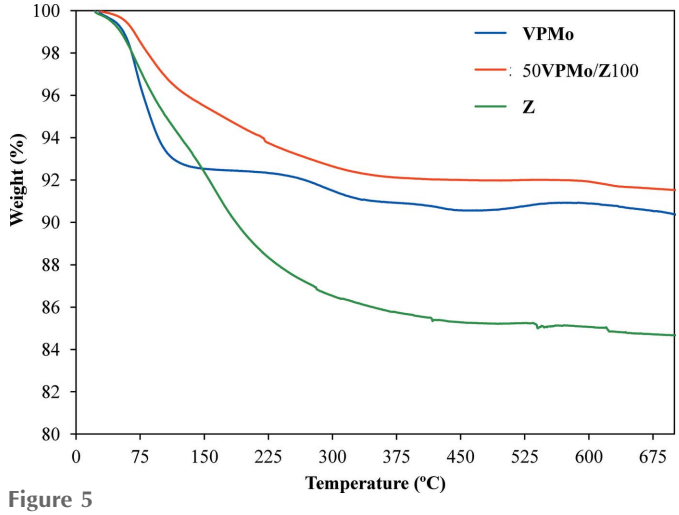


**Figure 5**
TGA curves of the **Z** support, the **VPMo** starting material and the 50**VPMo**/**Z**100 catalyst.

caused by the introduction of vanadium(V) in the primary structure of the Keggin-type phosphomolybdate anion facilitates decomposition of the cluster framework at lower temperatures through the output of $VO_x$ units toward the surface sites of the secondary structure, which would involve partial decomposition of the Keggin-type species into lacunary fragments and oxide phases (Mestl *et al.*, 2001; Molinari *et al.*, 2011). This behaviour is likely to contribute to the observation of $MoO_3$ and $V_2O_5$ in the DRIFT spectrum of the 50**VPMo**/**Z**300 sample.

**3.1.4. Thermogravimetric analysis**. The TGA curves of the **Z** support, the **VPMo** starting material and the 50**VPMo**/**Z**100 catalyst are compared in Fig. 5. The curve of **Z** shows two mass-loss stages that extend from room temperature to *ca* 150 °C, and from this temperature up to *ca* 400 °C. The former originates from the release of physisorbed water, whereas the latter corresponds to the transformation of the $Zr(OH)_4$ hydrogel obtained from co-precipitation procedures into $ZrO_2$, with associated loss of water molecules formed upon condensation. Similar features have been described previously by other authors (Wang *et al.*, 2001). In the case of the **VPMo** precursor, thermal decomposition takes place through four different stages. An initial mass loss that extends up to 200 °C and originates from the partial release of the crystallization water molecules (24 out of the 32 per POM cluster present in the starting material; see Mestl *et al.*, 2001) leads to the partially dehydrated $H_4PMo_{11}VO_{40}{\cdot}8H_2O$ phase, which undergoes loss of the remaining crystallization water molecules and partial decomposition with associated reduction of $V^V/Mo^{VI}$ centres to $V^{IV}/Mo^V$ in the temperature range from 200 to 500 °C. The subsequent mass gain that takes place between 500 and 600 °C can be then attributed to the reoxidation of the previously reduced metal atoms (Dimitratos & Védrine, 2006), whereas the final mass loss above 600 °C is related to the full breakdown of the Keggin-type framework with consequent release of water molecules originating from the protons of the HPA species (Bardin *et al.*, 1998).

Regarding the 50**VPMo**/**Z**100 sample, its TGA curve also displays two main mass-loss stages that somehow resemble those found separately in the **Z** support and the **VPMo** starting material. Nevertheless, it must be noted that the overall mass loss in the catalyst is much lower than those observed for the individual support and HPA components and this fact indicates that a strong **Z**/**VPMo** interaction is established during the impregnation procedure, which would involve the loss of hydroxy groups of the $Zr(OH)_4$ hydrogel upon condensation with the protons of the HPA species, as well as a decrease in the hydration sphere of the **VPMo** clusters to maximize the contact with the surface of the support.

**3.1.5. Catalytic activity**. (*a*) *Assessment of the optimal supported catalyst: VPMo loading and calcination temperature*. To determine the most suitable amount of catalytically active **VPMo** species that should be loaded into the **Z** support for achieving the heterogeneous catalyst with the highest activity in the $H_2O_2$-based oxidation of adamantane at 75 °C, a set of catalytic tests were performed using 0.1 g of four different *x***VPMo**/**Z**100 catalysts with **VPMo** mass percentages of $x$ = 5, 10, 25 and 50 wt%. As shown in Fig. 6, a conversion of only 11% is achieved after 6 h when the model reaction is carried out using the support only and in the absence of any catalyst, which justifies the need for introducing a suitable catalyst into the system for activating the oxidant $H_2O_2$. Our results indicate that all the catalysts tested are active in the model reaction and result in conversions of adamantane that increase almost linearly with the amount of supported **VPMo**, in such a way that they go from a reasonable *ca* 25% for the sample with the lowest POM loading (5**VPMo**/**Z**100) to a remarkable *ca* 90% for that with the highest amount of supported HPA

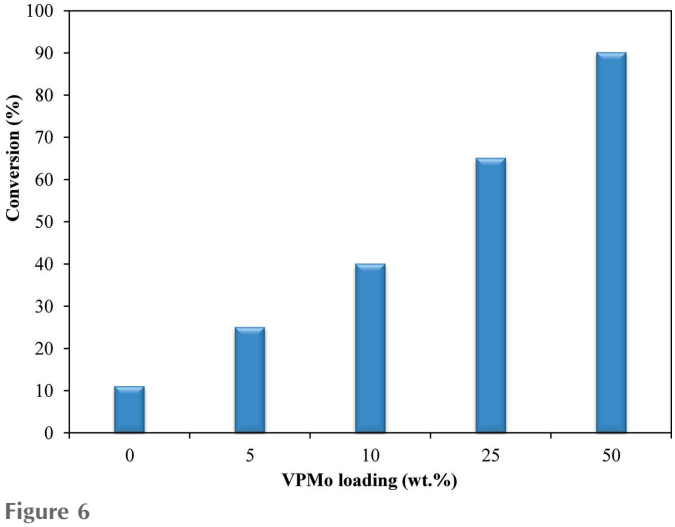


**Figure 6**
Conversion in the $H_2O_2$-based oxidation of adamantane (30 mmol of $H_2O_2$; 0.184 mmol of adamantane; 10 ml of acetonitrile; 75 °C, 6 h) catalysed by 0.1 g of *x***VPMo**/**Z**100 as a function of the **VPMo** loading (*x*).

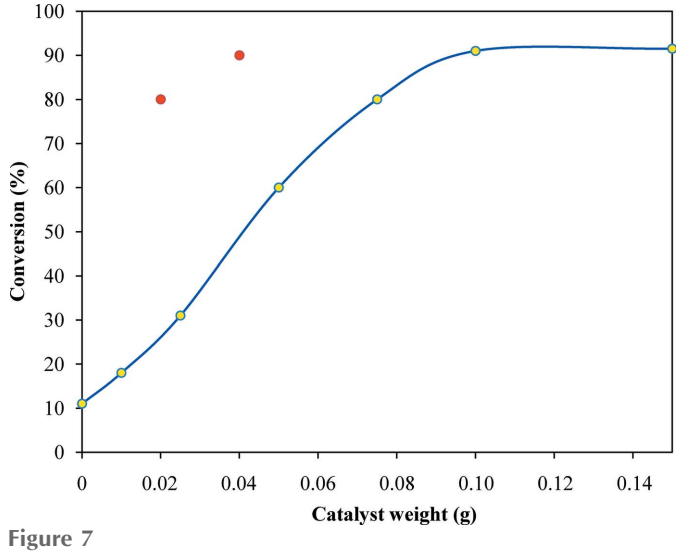


**Figure 7**
Conversion in the $H_2O_2$-based oxidation of adamantane (30 mmol of $H_2O_2$; 0.184 mmol of adamantane; 10 ml of acetonitrile; 75 °C, 6 h) catalysed by 50**VPMo**/**Z**100 (yellow) or unsupported **VPMo** (red; see Martín-Caballero *et al.*, 2016) as a function of the amount of catalyst.

**Table 2**
Leaching of supported **VPMo**, conversion and selectivity of the reaction products in the $H_2O_2$-based oxidation of adamantane (30 mmol of $H_2O_2$; 0.184 mmol of adamantane; 10 ml of acetonitrile; 75 °C, 6 h) catalysed by 0.1 g of 50**VPMo**/Z*t* (*t* = 100, 300 °C) through four consecutive runs.

| | Run | Leaching (wt%)[a] | Conversion (%) | Selectivity (%)[b] | | | |
|---|---|---|---|---|---|---|---|
| | | | | P1 | P2 | P3 | Others |
| 50**VPMo**/Z100 | 1 | 60 | 90 | 45 | 30 | 11 | 13 |
| | 2 | 15 | 65 | 38 | 41 | 14 | 6 |
| | 3 | 5 | 28 | 40 | 60 | - | - |
| | 4 | 3 | 13 | 41 | 59 | - | - |
| 50**VPMo**/Z300 | 1 | 21 | 85 | 33 | 31 | 10 | 25 |
| | 2 | 7 | 76 | 35 | 42 | 22 | - |
| | 3 | 3 | 53 | 39 | 53 | 7 | - |
| | 4 | 1 | 28 | 43 | 56 | 6 | - |

Notes: (*a*) with respect to the initial mass of supported **VPMo** (50 mg); (*b*) P1 is 1-adamantanol, P2 is 2-adamantanone, P3 is 2-adamantanol and 'Others' are 1,3-adamantanediol, 5-hydroxy-2-adamantanone and 1,3,5-adamantanetriol.

species (50**VPMo**/**Z**100). The latter catalyst has been shown as the most active within the series and has thus been selected as the most suitable for carrying out the following studies.

To find the minimum quantity of catalyst needed to achieve the highest conversion possible, a second set of catalytic tests was performed using different amounts of the 50**VPMo**/**Z**100 sample. The results depicted in Fig. 7 show that the oxidation process achieves higher conversions with an increasing amount of 50**VPMo**/**Z**100, as expected, but this trend develops only up to a quantity of 0.1 g of the catalyst, above which a plateau of around 90% of conversion is maintained. It is worth remarking that this level achieved with 0.1 g of 50**VPMo**/**Z**100 containing 0.05 g of the **VPMo** species compares very nicely to the conversion afforded by 0.04 g of the unsupported **VPMo** starting material catalyzing the oxidation reaction in the homogeneous phase, which demonstrates that the HPA clusters are very well dispersed across the **Z** support and that the adamantane substrate finds very good accessibility toward such catalytically active sites.

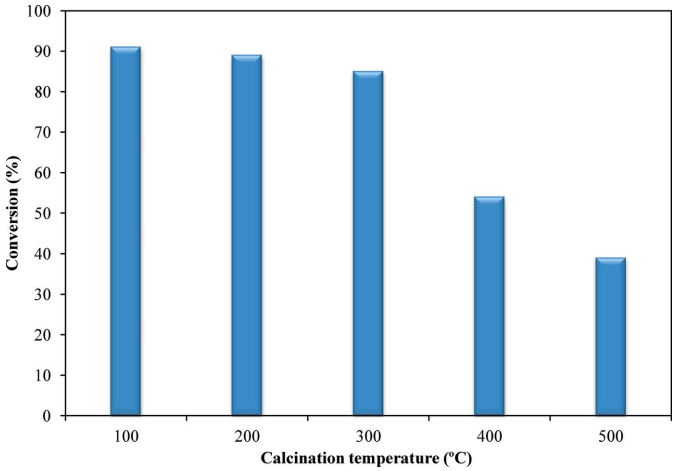


**Figure 8**
Conversion in the $H_2O_2$-based oxidation of adamantane (30 mmol of $H_2O_2$; 0.184 mmol of adamantane; 10 ml of acetonitrile; 75 °C, 6 h) catalysed by 0.1 g of 50**VPMo**/**Z***t* as a function of the calcination temperature (*t*).

To explore whether thermal treatment has any potential effect on the catalytic activity of our materials, a third set of catalytic tests were carried out using 0.1 g of 50**VPMo**/**Z***t* samples calcined at temperatures of *t* = 100, 200, 300, 400 and 500 °C. As shown in Fig. 8, the conversion of adamantane tends to lower with a raising of the calcination temperature. This decrease in the activity is subtle among those catalysts calcined in the temperature range from 100 to 300 °C (conversions of *ca* 90 and 85%, respectively), but becomes pronounced for those materials calcined at higher temperatures, in such a way that the conversion drops to *ca* 55% for the 50**VPMo**/**Z**400 sample and to *ca* 40% for 50**VPMo**/**Z**500. The low catalytic activity for the latter two materials is in full agreement with the partial decomposition of the Keggin-type framework observed by PXRD and DRIFT experiments for those samples calcined at temperatures higher than 300 °C (see above).

(*b*) *Study of the selectivity and reusability of the catalysts*. The 50**VPMo**/**Z**100 and 50**VPMo**/**Z**300 samples have been selected to explore the selectivity and reusability of our catalysts. Table 2 lists the conversions and the distributions of the reaction products afforded by 0.1 g of such samples in the oxidation of adamantane by $H_2O_2$ in acetonitrile at 75 °C through four successive reaction runs of 6 h each without any intermediate catalyst regeneration stage between consecutive catalytic cycles. For both samples, the catalytic activity decreases and the conversion becomes lower after each cycle, but this decrease is significantly more pronounced for the 50**VPMo**/**Z**100 catalyst. This behaviour originates from the leaching of the catalytically active **VPMo** clusters from the **Z** support toward the reaction medium, which could be observed qualitatively on the basis of the solution acquiring a yellowish colour characteristic of the **VPMo** species during the reaction. To quantify the amount of leached **VPMo** species from our **VPMo**/**Z** materials through several consecutive oxidation cycles, the solutions obtained upon filtration of the solid catalyst from the reaction media were analysed by UV–Vis spectroscopy after completion of each of the reaction runs. The corresponding spectra are compiled in Fig. S4 in the supporting information and the quantitative results on the **VPMo** leaching are listed in Table 2. The 50**VPMo**/**Z**100 sample shows the highest initial amount of leached **VPMo** species, which quickly decreases as more reaction cycles are accumulated. In contrast, the greater persistence of catalytic activity for the sample calcined at higher temperatures (50**VPMo**/**Z**300) is most likely associated with a stronger interaction between the **VPMo** clusters and the surface of the **Z** support that hampers leaching of the catalytically active units to some extent and, accordingly, with the significantly lower amount of leached **VPMo** determined after completion of the first reaction run.

The data in Table 2 show that the initial catalytic cycles in which the highest conversions are achieved result in the lowest selectivity as complex mixtures of 1-adamantanol (P1 in Table 2) and 2-adamantanone (P2 in Table 2) with low-to-trace yields of a great variety of other oxidation products (*e.g.* 2-adamantanol, 1,3-adamantanediol *etc.*) are obtained. In

contrast, the distribution of oxidation products narrows for the later catalytic cycles with the lowest conversions, in such a way that the mixture is limited to just P1 and P2 as the minor and major components, respectively (*ca* 40:60 ratio), with small amounts of 2-adamantanol also present in the case of 50**VPMo**/**Z**300. It must be pointed out in this context that the relative reactivities of the H atoms at the secondary and tertiary C atoms of adamantane (sites 1 and 2) have previously been reported to be nearly similar (Süss-Fink *et al.*, 2001). Thus, the differences found for the selectivity in our work should not originate in principle from any difference between the reactivity of the two sites. Therefore, high conversions associated with high catalytic activities appear to lead to overoxidation of the initial products P1 and P2, and hence to a wide distribution of reaction products and consequent low selectivity, whereas the catalysts are not able to overoxidize the initial mixture of P1 and P2 under lower activity conditions, thus resulting in significantly higher selectivity. To gain further insight into this aspect, the evolution of the selectivity toward P1 with adamantane conversion was studied for the 50**VPMo**/**Z**300 sample through the first (fresh catalyst) and second (reused catalyst) reaction runs. The results in Fig. S6 in the supporting information show that the selectivity toward P1 gradually decreases after 1 h of reaction as the conversion of adamantane increases for the fresh catalyst, whereas in the case of the reused sample, the selectivity is maintained at nearly similar values during the whole adamantane conversion process. These results are consistent with the fact that, once the initial products P1 and P2 are formed, they progress to overoxidation for the fresh catalyst with the highest activity and remain nearly intact for the reused sample. It is also worth noting that while P1 predominates in the initial mixture of products and its yield is maintained nearly constant throughout the four reaction runs, the selectivity of the tested catalysts turns toward P2 with an increasing number of catalytic cycles as its yield increases continuously and becomes the major product of the oxidation reaction. Regarding the influence of the thermal treatment on the catalyst performance, the data in Table 2 indicate that selectivity tends to weaken with increasing calcination temperature as the yields of 2-adamantanol and other overoxidized products are always higher for 50**VPMo**/**Z**300 than for 50**VPMo**/**Z**100 in all reaction runs, in good agreement with the highest catalytic activity shown by the former sample.

To evaluate the reusability of the catalysts in successive runs, both 50**VPMo**/**Z**100 and 50**VPMo**/**Z**300 were recovered after performing the first (**C1**) and fourth (**C4**) reaction runs, and were analysed by TGA experiments (Fig. 9). For both used samples, the TGA curves upon completion of the first (**C1**) and fourth (**C4**) reaction runs showed additional mass-loss stages at higher temperatures than those exhibited by the fresh catalysts. Thus, the additional mass loss that the **C1** and **C4** recovered samples undergo from *ca* 100 to 250 °C can be correlated with the removal of adamantane adsorbed at the catalyst surface during the reaction (the total combustion of adamantane takes place at *ca* 170 °C), while that observed above 500 °C most likely corresponds to the elimination of reaction products with higher molecular weights that are strongly retained at the catalyst upon completion of the catalytic cycle. This is in good agreement with the fact that the latter mass-loss stage becomes larger as the number of consecutive reaction runs increases. It is also worth noting that the overall mass loss is, in all cases, significantly more relevant for 50**VPMo**/**Z**100 than for 50**VPMo**/**Z**300 (45 *versus* 25% upon completion of the **C4** cycle). Taking into account that the former sample leads to a more pronounced decrease in conversion through consecutive reaction runs than the latter, such a loss of catalytic activity might also be attributable to a larger progressive accumulation of reaction products and the consequent blocking of active sites at the catalyst surface beyond the leaching effect commented on above.

### 3.2. Characterization of the catalysts obtained by the sol-gel method

**3.2.1. Porous texture**. The $N_2$ adsorption–desorption isotherms of the 50**VPMo**/**ZG***t* catalysts calcined at temperatures

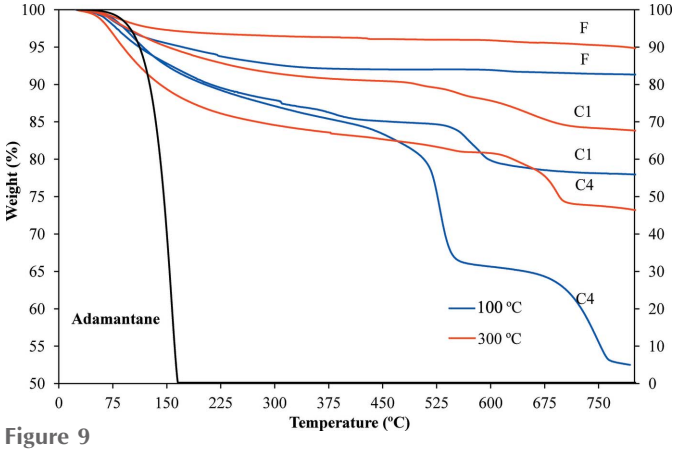


**Figure 9**
Comparison between the TGA curves of the fresh 50**VPMo**/**Z**100 and 50**VPMo**/**Z**300 catalysts (**F**) and those recovered after the first (**C1**) and last reaction runs (**C4**).

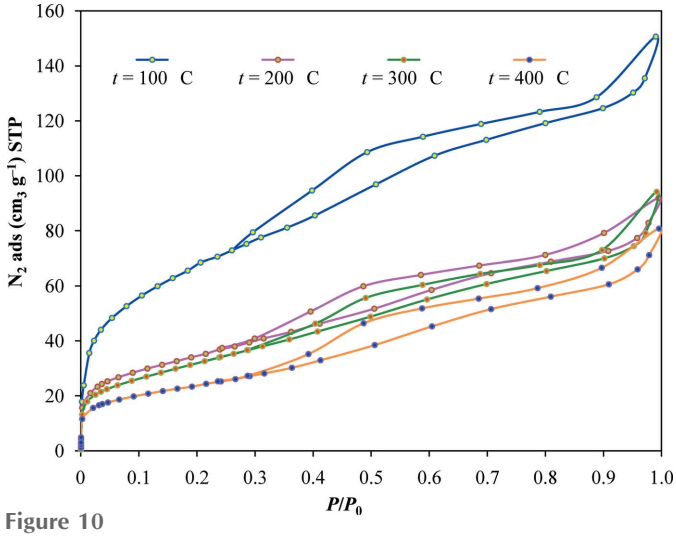


**Figure 10**
$N_2$ adsorption–desorption isotherms at −196 °C of the 50**VPMo**/**ZG***t* catalysts (*t* = 100–400 °C).

Table 3
Textural properties of 50**VPMo**/**ZG***t* catalysts obtained by the sol-gel method.

| | $V_{N2}$ (cm$^3$ g$^{-1}$) | $V_{CO2}$ (cm$^3$ g$^{-1}$) | $V_{meso}$ (cm$^3$ g$^{-1}$) | $V_T$ (cm$^3$ g$^{-1}$) | SBET (m$^2$ g$^{-1}$) |
|---|---|---|---|---|---|
| **ZG**100 | 0.19 | 0.09 | 0.01 | 0.20 | 330 |
| **ZG**200 | 0.11 | 0.07 | 0.01 | 0.12 | 195 |
| **ZG**300 | 0.09 | 0.04 | 0.01 | 0.10 | 142 |
| **ZG**400 | 0.05 | 0.03 | 0.03 | 0.08 | 80 |
| 50**VPMo**/**ZG**100 | 0.14 | 0.05 | 0.06 | 0.20 | 240 |
| 50**VPMo**/**ZG**200 | 0.07 | 0.03 | 0.05 | 0.12 | 122 |
| 50**VPMo**/**ZG**300 | 0.06 | 0.03 | 0.04 | 0.10 | 111 |
| 50**VPMo**/**ZG**400 | 0.05 | 0.02 | 0.05 | 0.10 | 86 |

$t$ = 100, 200, 300 and 400 °C are shown in Fig. 10, while the values of the parameters that define their textural properties, together with those of the corresponding **ZG***t* supports, are listed in Table 3. The samples prepared following the sol-gel synthetic procedure appear to display a larger porosity than those obtained from impregnation, as revealed by a comparison of the textural properties of 50**VPMo**/**ZG**100 with those of the 50**VPMo**/**Z**100 analogue, which did not show any type of porosity. Moreover, the development of the pore-size distributions in the 50**VPMo**/**ZG***t* catalysts is also modified with respect to that found for the samples obtained from impregnation according to the different shapes of the isotherms. The isotherms of the 50**VPMo**/**ZG***t* catalysts are of type IV, according to IUPAC classification (Thommes *et al.*, 2015), and they all display H2-type hysteresis loops, which are characteristic of inorganic mesoporous solids (de Boer *et al.*, 1958). Calcination of the samples at temperatures above 100 °C does not modify the isotherm shape, but produces a significant reduction in the adsorption capacity that takes place mainly at relatively low pressures ($P/P_0 < 0.2$), which is indicative of a decrease in the microporous volume.

The values of the textural properties given in Table 3 show that, even for a POM loading as high as 50 wt% that can only contribute with a significant amount of 'inert' weight to the porous texture, the **ZG**-supported **VPMo** catalysts obtained from the acid hydrolysis of a molecular zirconium(IV) precursor into a $Zr(OH)_4$ hydrogel in the presence of the HPA species contain a total porous volume nearly identical to that of the pristine **ZG** supports prepared by such a sol-gel method. Moreover, these values also indicate that the decrease of porosity with increasing calcination temperature commented on above is exclusively related to the thermal behaviour of the **ZG** support, as the trend through which the values of its textural properties lower from 100 to 400 °C is very similar to that found for the **ZG**-supported **VPMo** samples, in such a way that the porosity displayed by the 50**VPMo**/**ZG**400 is even slightly higher than that of the corresponding pristine **ZG**400 support. The combination of all of these observations reveals that the **VPMo** clusters are very well integrated into the structure of the **ZG** support through the sol-gel preparative method, thereby facilitating the development of porosity in the resulting solid material and stabilizing its porous nature against contraction during calcination.

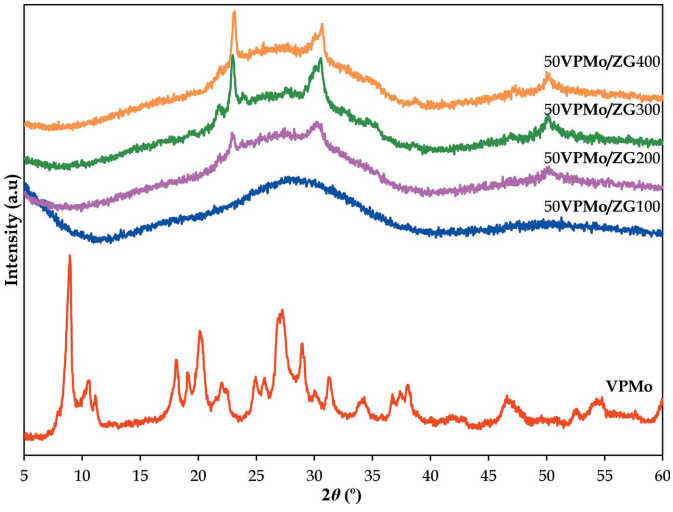


Figure 11
PXRD patterns of calcined 50**VPMo**/**ZG***t* samples ($t$ = 100–400 °C).

**3.2.2. Powder X-ray diffraction**. PXRD experiments on the 50**VPMo**/**ZG***t* catalysts calcined at temperatures $t$ = 100, 200, 300 and 400 °C support the consideration of an optimal integration of the **VPMo** species into the structure of the zirconia matrix (Fig. 11). The absence of the main diffraction maximum of the **VPMo** starting material ($2\theta$ = 8.9°) in any of the PXRD patterns of the 50**VPMo**/**ZG***t* samples indicates that **VPMo** is very well dispersed in the **ZG** support and does not form any particulate aggregate large enough to be structurally detected in spite of the high POM loading of the catalysts. Compared with the corresponding materials prepared following the impregnation method, the PXRD patterns of the 50**VPMo**/**ZG***t* catalysts exhibit hardly any diffraction maxima, which reveals the nature of these solids as substantially more amorphous. The appearance of defined diffraction maxima can only be noticed when the 50**VPMo**/**ZG** material is calcined at temperatures higher than 200 °C. The signals centred at $2\theta$ values of *ca* 30 and 50° correspond to the tetragonal $ZrO_2$ phase (JCPDS 80-2155C), whereas the emergence of a major diffraction peak at $2\theta$ = 23° indicates progressive formation of the $\beta$-$MoO_3$ phase (Molinari *et al.*, 2011) from partial decomposition of the **VPMo** clusters. In all the 50**VPMo**/**ZG***t* samples, these diffraction maxima are substantially wider and less intense than those observed for the corresponding 50**VPMo**/**Z***t* analogues, which indicates a higher thermal stability of the **VPMo** species, most likely due to their better integration into the structure of the support.

**3.2.3. Diffuse reflectance IR Fourier transform spectroscopy**. To investigate whether the Keggin-type framework of the **VPMo** clusters is preserved during the sol-gel synthetic procedure and subsequent thermal treatments, DRIFT spectra were recorded for the 50**VPMo**/**ZG**100 and 50**VPMo**/**ZG**300 samples (Fig. 12). The most significant feature in these spectra is the presence of a broad band centred at *ca* 850 cm$^{-1}$ that originates from the $\nu$(Zr—O) vibration mode (Hernández Enríquez *et al.*, 2009), the intensity of which increases with the calcination temperature and is always higher than that found in the spectra of the corresponding 50**VPMo**/**Z***t* analogues. In

Table 4
Leaching of supported **VPMo**, conversion and selectivity of the reaction products in the $H_2O_2$-based oxidation of adamantane (30 mmol of $H_2O_2$; 0.184 mmol of adamantane; 10 ml of acetonitrile; 75 °C, 6 h) catalysed by 0.1 g of 50**VPMo**/**ZG***t* calcined at *t* = 100 (first and fourth reaction runs) and *t* = 300 °C (throughout four consecutive runs).

| | Run | Leaching (wt%)[a] | Conversion (%) | Selectivity (%)[b] | | | |
|---|---|---|---|---|---|---|---|
| | | | | P1 | P2 | P3 | Others |
| 50**VPMo**/**ZG**100 | 1 | 43 | 87 | 22 | 13 | 9 | 56 |
| | 4 | 3 | 40 | 35 | 46 | 10 | 9 |
| 50**VPMo**/**ZG**300 | 1 | 10 | 90 | 17 | 10 | 7 | 66 |
| | 2 | 3 | 85 | 30 | 13 | 12 | 45 |
| | 3 | - | 97 | 13 | 6 | 5 | 76 |
| | 4 | - | 98 | 3 | 2 | 1 | 94 |

Notes: (*a*) with respect to the initial mass of supported **VPMo** (50 mg). (*b*) P1 is 1-adamantanol, P2 is 2-adamantanone, P3 is 2-adamantanol and 'Others' are 1,3-adamantanediol, 5-hydroxy-2-adamantanone and 1,3,5-adamantanetriol.

contrast to what was observed for the catalysts loaded with 50 wt% of **VPMo** by impregnation and calcined at 100 and 300 °C, the DRIFT fingerprint of the primary Keggin structure of the **VPMo** species (Mestl *et al.*, 2001) can be hardly noticed in the spectrum of 50**VPMo**/**ZG**100 and nearly fades away for 50**VPMo**/**ZG**300 due to being masked in the 750–1000 $cm^{-1}$ range by the contribution of the support. The presence of the HPA species can only be inferred from the peaks at *ca* 1080 and 980 $cm^{-1}$ originating from the $\nu_{as}(P{-}O_a)$ and $\nu_{as}(Mo{=}O_d)$ vibration modes, respectively. This fact confirms the **VPMo** clusters as being very well dispersed or even integrated on a molecular scale within the **ZG** matrix, so that the intensity of its DRIFT fingerprint is attenuated compared to the case in which nanoparticulated **VPMo** aggregates are merely supported at the **ZG** surface.

**3.2.4. Thermogravimetric analysis**. The TGA curves of the **ZG** support and the 50**VPMo**/**ZG**100 catalyst are displayed in Fig. 13. The overall mass losses that both samples undergo with increasing temperature are significantly larger than those observed for the corresponding analogues obtained from impregnation (30 *versus* 16% in the case of the **ZG** and **Z** supports, for example). Going from a synthetic method based on impregnation to a procedure involving trapping the **VPMo** species in the zirconia matrix as the latter is generated *in situ* also results in a modification of the different mass-loss stages. Thus, the first stage up to 200 °C corresponds to the removal of water and ethanol molecules occluded within the gel, whereas the second stage originates from two different processes: (i) the combustion of residual organic matter (*n*-butoxy groups) in the 200–300 °C range, and (ii) the transformation of the $Zr(OH)_4$ hydrogel into $ZrO_2$ with consequent release of condensation water molecules that takes place from 200 to 400 °C (Wang *et al.*, 2001). In the case of the 50**VPMo**/**ZG**100 catalyst, an additional mass loss corresponding to the thermal decomposition of the primary Keggin-type framework is observed in the 400–500 °C range.

**3.2.5. Catalytic activity, selectivity and reusability**. The catalytic performances of the 50**VPMo**/**ZG**100 and 50**VPMo**/**ZG**300 samples in the oxidation of adamantane were studied under the same experimental conditions as those applied for the samples obtained by impregnation, and the results are collected in Table 4. Both catalysts show initial conversions similar to those of the corresponding analogues obtained by impregnation, but poorer selectivities as the initial yields of P1 and P2 are nearly half of those afforded by 50**VPMo**/**Z**100 and 50**VPMo**/**Z**300, in such a way that the main fraction of the mixture of reaction products corresponds to the overoxidized species. The catalytic performance of 50**VPMo**/**ZG**100 follows a trend that resembles that of the catalysts obtained from impregnation, that is, the conversion decreases with the number of consecutive reaction runs while the selectivity increases, in such a way that the mixture of reaction products for the **C4** cycle is dominated by P1 and P2 as the minor and major components, respectively (35:45 ratio). Moreover, the leaching of the **VPMo** species into the reaction medium is initially high, as for the corresponding impregnation analogue, which is indicative of the weak interaction established between the POM clusters and the support when the sample is calcined at low temperatures. However, this decrease of activity originating from the progressive loss of the catalyti-

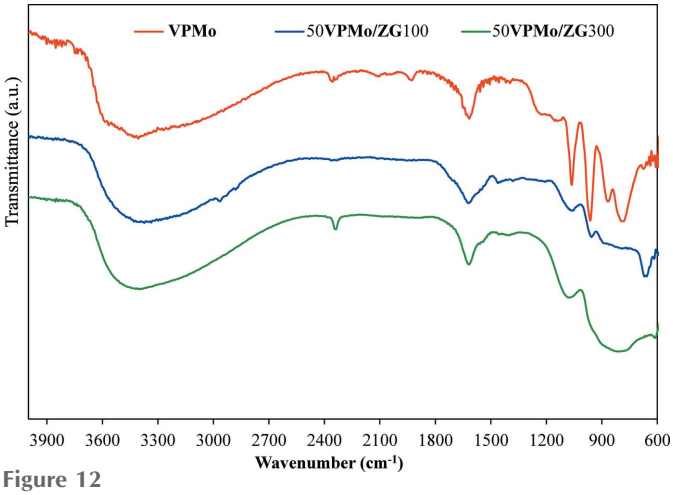


Figure 12
DRIFT spectrum of **VPMo** compared to those of the 50**VPMo**/**ZG** samples calcined at 100 and 300 °C.

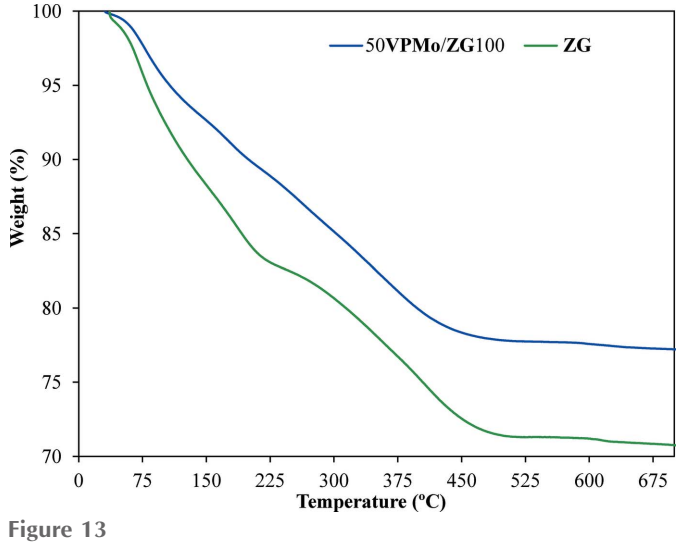


Figure 13
TGA curves of the **ZG** support and the 50**VPMo**/**ZG**100 sample.

cally active species throughout successive runs is not as pronounced as that found for the 50**VPMo**/**Z**100 analogue and, consequently, the distribution of reaction products upon completion of the **C4** cycle is not limited to just P1 and P2, but small amounts of P3 and other overoxidized products are still obtained.

In contrast, the catalytic performance of 50**VPMo**/**ZG**300 develops in a completely different manner. The catalyst does not undergo any deactivation and the conversion is maintained around 90% throughout the four consecutive reaction runs, with even a slight increase to near full conversion (98%) during the last cycle, *i.e.* **C4**. Accordingly, leaching of the **VPMo** species into the reaction media is almost negligible, but for a little amount during the first catalytic cycle. As discussed above for the TG and DRIFTS experiments, calcination at temperatures higher than 100 °C promotes the progressive transformation of the $Zr(OH)_4$ hydrogel formed upon acid hydrolysis of a molecular zirconium(IV) precursor into $ZrO_2$ and, considering the initial very high dispersion of the **VPMo** species in the supporting matrix, such a thermally triggered transformation must result in the clusters being tightly entrapped within the structure of the final oxide, thereby ensuring retention of porosity for a suitable access of the substrate toward the catalytically active sites and preventing any loss of the latter during the reaction. In line with this increase in catalytic activity with the number of reaction runs, the selectivity is fully lost and only negligible amounts of P1 and P2 (yields lower than 5%) are found in the mixture of products obtained from the catalytic **C4** cycle, which is in turn essentially composed of a great variety of other overoxidized species.

To explore in depth the development of the catalytic performance of the 50**VPMo**/**ZG**300 sample, the catalyst was further analysed by TGA (Fig. 14) and DRIFTS (Fig. 15) experiments upon completion of cycles **C1** and **C4**. As observed for the 50**VPMo**/**Z**300 analogue, the overall mass loss that the catalyst undergoes with temperature becomes larger with the number of reaction runs due to the progressive accumulation of both nonreacted adamantane substrate and reaction products (eliminated by combustion at temperatures below and above *ca* 300 °C, respectively). The magnitudes of the overall mass losses associated with the **C1** and **C4** recovered samples are similar for both 50**VPMo**/**Z**300 and 50**VPMo**/**ZG**300, regardless of the preparation procedures being based on impregnation or sol-gel methods. In the former case, this fact contributed to the loss of catalytic activity, whereas for the latter, the accumulation of organic matter has no influence on the conversions achieved during the reaction runs. The occurrence of such opposite behaviours can be related to the differences found in the textural properties of both samples: the lack of porosity of 50**VPMo**/**Z**300 makes the progressive accumulation of organic matter at its surface block the catalytically active sites, whereas in 50**VPMo**/**ZG**300, access of the substrate to the immobilized **VPMo** species cannot be hampered by the retained organic molecules due to the mesoporous nature of the **ZG** support. Analysis of the porous texture of 50**VPMo**/**ZG**300 confirms this hypothesis as it still displays a considerable adsorption capacity upon completion of catalytic cycle **C4** (see Fig. S5 in the supporting information). For comparison, the porosity of 50**VPMo**/**ZG**100 drops dramatically when recovered from the first reaction run and disappears fully when the next cycle is complete. These results are in full agreement with the different trends through which the conversions afforded by 50**VPMo**/**ZG**300 and 50**VPMo**/**ZG**100 evolve throughout the four consecutive runs.

Nevertheless, the results above cannot explain why the catalytic activity of 50**VPMo**/**ZG**300 tends to increase with the number of reaction runs. The DRIFT analysis of this sample upon catalysing the $H_2O_2$-based oxidation of adamantane reveals the appearance of an additional signal at *ca* 880 $cm^{-1}$, the intensity of which increases when going from cycle **C1** to **C4**. This signal can be assigned to the formation of O—O

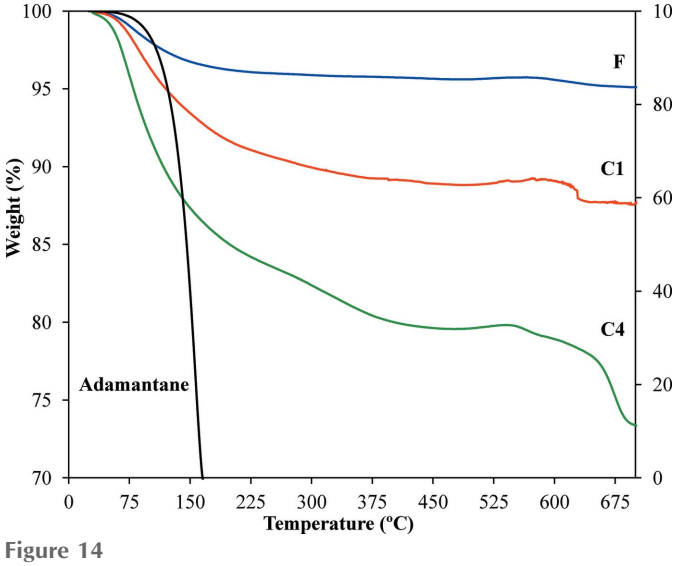


**Figure 14**
Comparison between the TGA curve of the fresh 50**VPMo**/**Z**300 catalyst (**F**) and those recovered after the first (**C1**) and last reaction runs (**C4**).

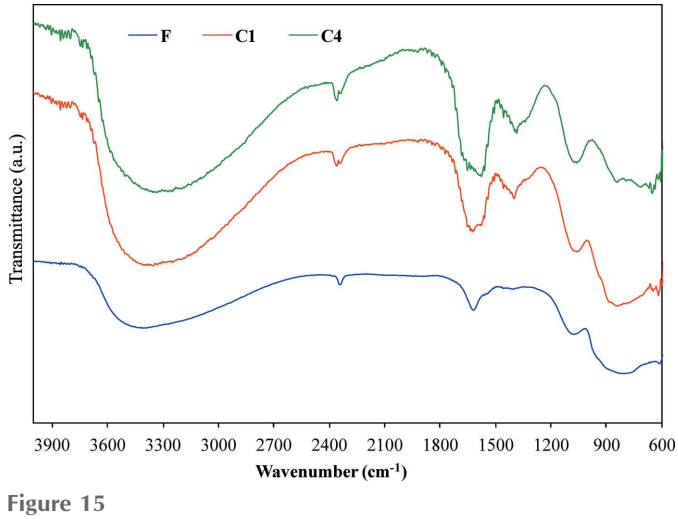


**Figure 15**
Comparison between the DRIFT spectrum of the fresh 50**VPMo**/**Z**300 catalyst (**F**) and those recovered after the first (**C1**) and last reaction runs (**C4**).

peroxo groups in the catalyst during the reaction (Dickman & Pope, 1994; Griffith, 1963). In close analogy to a variety of molecular oxidation catalysts based on transition-metal complexes acting under homogeneous conditions (Antonelli *et al.*, 1988; Mizuno *et al.*, 2005), the activation of the $H_2O_2$ oxidant by heterogeneous catalysts based on supported POM clusters has been previously confirmed to originate from the formation of peroxometallic POM intermediates at the catalyst surface (Alcañiz-Monge *et al.*, 2014) and, therefore, the increase in activity with the number of cycles observed for 50**VPMo**/**ZG**300 is most likely attributable to a progressive increase in the number of active peroxo-**VPMo** species when going from the first to the fourth reaction run. Monitoring of the conversion performed on the filtrate obtained upon separation of different solid catalysts from the reaction mixture after just 1 h of reaction (Fig. S7 in the supporting information) confirms that the oxidation of adamantane is mainly catalysed by the immobilized **VPMo** species in the case of the sol-gel synthesized 50**VPMo**/**ZG**300 sample. This DRIFTS analysis also shows the emergence of a second additional band at 1398 $cm^{-1}$ and the signals at 1623 and 3600–2400 $cm^{-1}$ becoming wider and more intense. These bands can be assigned to vibrations of C═O, O—H and –$CH_2$ groups, respectively, which supports the fact of that reaction products, such as adamantanol or adamantanone, are retained and accumulated at the catalyst surface.

## 4. Conclusions

A series of zirconia-supported 11-molybdovanadophosphoric acid oxidation catalysts with different polyoxometalate loadings have been prepared following two different synthetic procedures, *i.e.* wet-impregnation and sol-gel, both involving a final calcination stage. The effect of the preparative method and thermal treatment on the performance of the catalysts in the oxidation of adamantane has been evaluated. Our results indicate that the most effective catalysts able to better maintain their activity throughout several consecutive reaction runs are those prepared by the sol-gel method, whereas those prepared by impregnation tend to deactivate faster but are the most selective in turn. The different textural properties developed by each synthetic method, as well as the differences in the dispersion of the heteropoly acid across the support and the interaction between both components, are at the origin of these opposite behaviours. The impregnation method results in essentially microporous solids, the porosity of which decreases with increasing heteropoly acid content, until being fully blocked for a polyoxometalate loading of 50 wt%. In contrast, the catalysts obtained by the sol-gel method display a mesoporous character with higher pore volumes and are able to maintain a certain adsorption capacity regardless of the amount of polyoxometalate loaded or the temperature at which the solid is calcined. The dispersion and integration of the clusters within the zirconia matrix appears to be substantially better for the catalysts obtained by the sol-gel method according to powder X-ray diffraction and diffuse reflectance IR Fourier transform spectroscopy experiments.

Our studies also indicate that the calcination temperature is an important parameter in the synthesis of heterogeneous catalysts based on immobilized heteropoly acids. The loss of catalytic activity has been found to originate in part from the leaching of heteropoly acid units from the support into the solution, but this process can be hindered to some extent by increasing the calcination temperature, which enhances the interaction between the heteropoly acid clusters and the support by transforming the latter from a $Zr(OH)_4$ hydrogel into $ZrO_2$. The progressive accumulation of reaction products at the catalyst surface also contributes to the loss of activity that the catalysts obtained from impregnation undergo by increasing the number of cycles, but does not affect the sol-gel materials due to their textural properties. In turn, the formation and accumulation of peroxo–polyoxometalate intermediates responsible for activating the $H_2O_2$ oxidant is the origin of the increase in the activity observed for the latter catalysts.

## Acknowledgements

All authors have given approval to the final version of this manuscript. There are no conflicts of interest to declare.

## Funding information

Funding for this research was provided by: Generalitat Valenciana (grant No. PROMETE/2018/076); Ministerio de Economía, Industria y Competitividad (grant No. CTQ2015–64801-R); Obra Social la Caixa, Fundación Caja Navarra and Universidad Pública de Navarra (contract to SR in the framework of the program 'Captación de Talento').

## References

Alcañiz-Monge, J., El Bakkali, B., Trautwein, G. & Reinoso, S. (2018). *Appl. Catal. B*, **224**, 194–3809.
Alcañiz-Monge, J., Trautwein, G. & Garcia-Garcia, A. (2014). *J. Mol. Catal. A*, **394**, 211–216.
Alcañiz-Monge, J., Trautwein, G. & Marco-Lozar, J. P. (2013). *Appl. Catal. A*, **468**, 432–441.
Alcañiz-Monge, J., Trautwein, G., Parres-Esclapez, S. & Maciá-Agulló, J. A. (2008). *Microporous Mesoporous Mater.* **115**, 440–446.
Antonelli, E., D'Aloisio, R., Gambaro, M., Fiorani, T. & Venturello, C. (1988). *J. Org. Chem.* **63**, 7190–7206.
Arichi, J., Eternot, M. & Louis, B. (2008). *Catal. Today*, **138**, 117–122.
Babou, F., Coudurier, G. & Vedrine, J. C. (1995). *J. Catal.* **152**, 341–349.
Bardin, B. B., Bordawekar, S. V., Neurock, M. & Davis, R. J. (1998). *J. Phys. Chem. B*, **102**, 10817–10825.
Boer, J. H. de (1958). *The Structure and Properties of Porous Materials*, edited by D. H. Everett & F. S. Stone, p. 68. London: Butterworths.
Boon, J. A., Levisky, J. A., Pflug, J. L. & Wilkes, J. S. (1986). *J. Org. Chem.* **51**, 480–483.
Bordoloi, A., Vinu, A. & Halligudi, S. B. (2007). *Appl. Catal. A*, **333**, 143–152.
Bossmann, S. H., Oliveros, E., Göb, S., Siegwart, S., Dahlen, E. P., Payawan, L., Straub, M., Wörner, M. & Braun, A. M. (1998). *J. Phys. Chem. A*, **102**, 5542–5550.
Brunauer, S., Emmett, P. H. & Teller, E. (1938). *J. Am. Chem. Soc.* **60**, 309–319.
Campbell, C. T. (2012). *Nat. Chem.* **4**, 597–598.

Cazorla-Amorós, D., Alcañiz-Monge, J. & Linares-Solano, A. (1996). *Langmuir*, **12**, 2820–2824.
Chang, J., Wang, A., Liu, J., Li, X. & Hu, Y. (2010). *Catal. Today*, **149**, 122–126.
Damyanova, S. & Fierro, J. L. G. (1998). *Chem. Mater.* **10**, 871–879.
Dickman, M. H. & Pope, M. T. (1994). *Chem. Rev.* **94**, 569–584.
Dimitratos, N. & Védrine, J. C. (2006). *J. Mol. Catal. A*, **255**, 184–192.
Dubinin, M. M. (1966). *Chemistry and Physics of Carbon*, Vol. 2, edited by P. L. Walker, pp. 51–120. New York: Marcel Dekker.
Endalew, A. K., Kiros, Y. & Zanzi, R. (2011). *Biomass Bioenergy*, **35**, 3787–3809.
Farhadi, S. & Zaidi, M. (2009). *Appl. Catal. A*, **354**, 119–126.
Goodman, D. W. (1995). *Chem. Rev.* **95**, 523–536.
Griffith, W. P. (1963). *J. Chem. Soc.* pp. 5345–5350.
Hernández Enríquez, J. M., Cortez Lajas, L. A., García Alamilla, R., Castillo Mares, A., Sandoval Robles, G. & García Serrano, L. A. (2009). *J. Alloys Compd*, **483**, 425–428.
Herzog, B., Wohlers, M. & Schlögl, R. (1997). *Mikrochim. Acta*, **14**, 703–704.
Kozhevnikov, I. V. (2002). In *Catalysts for Fine Chemical Synthesis*, Vol. 2, *Catalysis by Polyoxometalates*. Chichester: John Wiley & Sons.
Leofanti, G., Padovan, M., Tozzola, G. & Venturelli, B. (1998). *Catal. Today*, **41**, 207–219.
Martín-Caballero, J., San José Wéry, A., Reinoso, S., Artetxe, B., San Felices, L., El Bakkali, B., Trautwein, G., Alcañiz-Monge, J., Vilas, J. L. & Gutiérrez-Zorrilla, J. M. (2016). *Inorg. Chem.* **55**, 4970–4979.
McGarvey, G. B. & Moffat, J. B. (1991). *J. Mol. Catal.* **69**, 137–155.
Mestl, G., Ilkenhans, T., Spielbauer, D., Dieterle, M., Timpe, O., Kröhnert, J., Jentoft, F., Knözinger, H. & Schlögl, R. (2001). *Appl. Catal. A*, **210**, 13–34.
Mizuno, N. & Kamata, K. (2011). *Chem. Rev.* **255**, 2358–2370.
Mizuno, N., Shu, D.-J., Han, W. & Kudo, T. (1996). *J. Mol. Catal. A*, **114**, 309–317.
Mizuno, N., Yamaguchi, K. & Kamata, K. (2005). *Coord. Chem. Rev.* **249**, 1944–1956.
Moffat, J. B. (2001). In *Metal–Oxygen Clusters: The Surface and Catalytic Properties of Heteropoly Oxometalates*. New York: Kluwer Academic Publishers.
Molinari, J. E., Nakka, L., Kim, T. & Wachs, I. E. (2011). *ACS Catal.* **1**, 1536–1548.
Noyori, R., Aoki, M. & Sato, K. (2003). *Chem. Commun.* pp. 1977–1986.
Parida, K. M. & Mallick, S. (2008). *J. Mol. Catal. A*, **279**, 104–111.
Patel, S., Purohit, N. & Patel, A. (2003). *J. Mol. Catal. A*, **192**, 195–202.
Pizzio, L. R., Cáceres, C. V. & Blanco, M. N. (1998). *Appl. Catal. A*, **167**, 283–294.
Pizzio, L. R., Vázquez, P. G., Cáceres, C. V. & Blanco, M. N. (2003). *Appl. Catal. A*, **256**, 125–139.
Popa, A., Sasca, V., Stefanescu, M., Kiš, E. & Marinković-Nedučin, R. (2006). *J. Serb. Chem. Soc.* **71**, 235–249.
Pope, M. T. & Müller, A. (1991). *Angew. Chem. Int. Ed. Engl.* **30**, 34–48.
Qiu, J., Wang, G., Zhang, Y., Zeng, D. & Chen, Y. (2015). *Fuel*, **147**, 195–202.
Rao, P. S. N., Venkateswara Rao, K. T., Sai Prasad, P. S. & Lingaiah, N. (2010). *Catal. Commun.* **11**, 547–550.
Rivera, T. S., Sosa, A., Romanelli, G. P., Blanco, M. N. & Pizzio, L. R. (2012). *Appl. Catal. A*, **443–444**, 207–213.
Rocchiccioli-Deltcheff, C. & Fournier, M. (1991). *J. Chem. Soc. Faraday Trans.* **87**, 3913–3920.
Shaabani, A. & Rezayan, A. H. (2007). *Catal. Commun.* **8**, 1112–1116.
Shinachi, S., Matsushita, M., Yamaguchi, K. & Mizuno, N. (2005). *J. Catal.* **233**, 81–89.
Song, I. K., Kitchin, J. R. & Barteau, M. A. (2002). *Proc. Natl Acad. Sci. USA*, **99**, 6471–6475.
Süss-Fink, G., Gonzalez, L. & Shul'pin, G. G. (2001). *Appl. Catal. A*, **217**, 111–117.
Tauster, S. J., Fung, S. C. & Garten, R. L. (1978). *J. Am. Chem. Soc.* **100**, 170–175.
Thommes, M., Kaneko, K., Neimark, A. V., Olivier, J. P., Rodríguez-Reinoso, F., Rouquerol, J. & Sing, K. S. W. (2015). *Pure Appl. Chem.* **87**, 1051–1069.
Tropecêlo, A. I., Casimiro, M. H., Fonseca, I. M., Ramos, A. M., Vital, J. & Castanheiro, J. E. (2010). *Appl. Catal. A*, **390**, 183–189.
Tsigdinos, G. A. & Hallada, C. J. (1968). *Inorg. Chem.* **7**, 437–441.
Wang, J. A., Valenzuela, M. A., Salmones, J., Vázquez, A., García-Ruiz, A. & Bokhimi, X. (2001). *Catal. Today*, **68**, 21–30.